Received May 31, 2018, accepted July 7, 2018, date of publication July 27, 2018, date of current version August 28, 2018.

Digital Object Identifier 10.1109/ACCESS.2018.2859782

A Novel 3D Non-Stationary Vehicle-to-Vehicle Channel Model and Its Spatial-Temporal Correlation Properties

QIUMING ZHU[1,2], (Member, IEEE), YING YANG[1], XIAOMIN CHEN[1], YI TAN[2], YU FU[2], CHENG-XIANG WANG[2,3], (Fellow, IEEE), AND WEIDONG LI[1]

[1]College of Electronic and Information Engineering, Nanjing University of Aeronautics and Astronautics, Nanjing 211106, China
[2]School of Engineering and Physical Sciences, Heriot-Watt University, Edinburgh EH14 4AS, U.K.
[3]State Key Laboratory of Mobile Communications, Southeast University, Nanjing 211189, China

Corresponding authors: Qiuming Zhu (zhuqiuming@nuaa.edu.cn) and Cheng-Xiang Wang (chxwang@seu.edu.cn)

This work was supported in part by the EU H2020 ITN 5G Wireless Project under Grant No. 641985, in part by the EU H2020 RISE TESTBED Project under Grant 734325, in part by the EPSRC TOUCAN Project under Grant EP/L020009/1, in part by the Natural Science Foundation of China under Grant 61631020 and 2013YQ200607, in part by the Fundamental Research Funds for the Central Universities under Grant NJ20160027, and in part by the Open Foundation for the Graduate Innovation of NUAA under Grant kfjj20170405.

ABSTRACT In this paper, a new non-stationary Vehicle-to-Vehicle (V2V) channel model is proposed. It could generate more smooth fading phase between the adjacent channel states and guarantee more accurate Doppler frequency, which is a great improvement comparing with those of the existing non-stationary geometry-based stochastic models (GBSMs) for V2V channels. Meanwhile, the spatial–temporal correlation function (STCF) as well as a temporal correlation function (TCF) and a spatial correlation function (SCF) are derived in details based on the power angle spectrums of both the mobile transmitter (MT) and mobile receiver (MR) following the Von Mises Fisher (VMF) distribution. Simulation results have demonstrated that the time-variant correlation properties of our proposed channel model have an excellent agreement with the theoretical results, which verifies the correctness of theoretical derivations and simulations. Finally, the TCF and stationary interval of the proposed model are verified by the measured results.

INDEX TERMS Non-stationary vehicle-to-vehicle (V2V) channel, geometry-based stochastic model (GBSM), Von Mises Fisher (VMF) distribution, spatial-temporal correlation properties.

I. INTRODUCTION

Multiple-input multiple-output (MIMO) technologies have attracted great research interest for their ability to improve the spectral efficiency and link reliability [1]–[4]. Massive MIMO has also been considered as one of key technologies for the fifth generation (5G) mobile communication systems [5]–[7]. However, the insufficient antenna space or lack of rich scattering would increase spatial-temporal correlations and degrade the performance of MIMO systems significantly [1]–[3]. Hence, the exploitation of spatial-temporal correlation properties has become a hot topic of evaluation and optimization for future communication systems.

The stationary geometry-based stochastic models (GBSMs) for the Vehicle-to-Vehicle (V2V) channel with the wide-sense stationary (WSS) assumption [8]–[10] have been widely accepted for the past decade. The time-invariant temporal correlation function (TCF) and the spatial correlation function (SCF) of these models were also studied in [8] and [9]. However, measurement results have shown that the WSS assumption is only valid for a short time interval [11] and the realistic V2V channels should have non-stationary characteristics such as time-variant spatial-temporal correlation properties [12].

Recently, several non-stationary GBSMs for V2V channels can be found in the literature [13]–[20]. By using the geometrical relationships of the scatterers with the given distributions, the SCF and TCF of these non-stationary GBSMs were studied by either simulations [13]–[18] or analytical methods [19], [20]. However, we have found that the output channel phases of aforementioned non-stationary V2V channel models in [13]–[20] are not accurate and this makes the corresponding output Doppler frequencies do not agree well with the theoretical ones [21]–[23]. Patzold *et al.* [24]

2169-3536 © 2018 IEEE. Translations and content mining are permitted for academic research only.
Personal use is also permitted, but republication/redistribution requires IEEE permission.
See http://www.ieee.org/publications_standards/publications/rights/index.html for more information.

and Dahech *et al.* [25] proposed a modified non-stationary channel model to overcome this shortcoming. Especially, in [24], the modified models were termed as Class A models, while the models in [13]–[20] were termed as Class B models. It should be mentioned that the proposed models in [24] and [25] were designed only for 2D scattering environments. Besides, the SCF and TCF for the proposed 2D non-stationary channel model have not been studied thoroughly due to the complex formula deduction. This paper aims to fill the above research gap. The major contributions and novelties of this paper are summarized as follows:

1) This paper proposes a novel 3D non-stationary GBSM for V2V channels under the 3D Von Mises Fisher (VMF) scattering environment. The proposed GBSM considers the scenarios of multiple bounces and can guarantee more realistic Doppler frequency or Doppler power spectrum density.

2) The correlation properties of the proposed GBSM are deeply investigated. The accurate and approximate expressions of the TCF and SCF are derived, which is a great improvement for those of the conventional non-stationary V2V GBSMs [13]–[20].

3) The proposed 3D non-stationary GBSM is validated by the measurements in [26] and [27] according to the TCF and stationary interval, respectively.

The remainder of this paper is organized as follows. Section II presents a new 3D non-stationary V2V GBSM as well as the time-variant channel parameters, such as the number of valid paths, angles of arrival (AoAs), and angles of departure (AoDs). In section III, the expressions of the SCF and TCF of the proposed model are derived. The numerical simulation results are performed and compared with the theoretical ones in Section V. Finally, the conclusions are given in Section VI.

II. A NOVEL GBSM FOR 3D NON-STATIONARY V2V CHANNEL MODEL

A. DESCRIPTION OF THE PROPOSED GBSM

Fig. 1 shows a typical V2V communication channel between the mobile transmitter (MT) equipped with S antennas and the mobile receiver (MR) equipped with U antennas. The channel between each pair of antenna elements includes multiple propagation paths and each path contains several clusters as given in Fig. 1. Since all clusters are random and time-variant under the V2V scenarios, it's very difficult to model all of them separately and accurately. For simplicity, the two-cluster approach in [28] and [29] is adopted in the proposed model. Only the first and last clusters denoted by A_n and Z_n, respectively, are modeled by their own locations and velocities. The rest of clusters between them are abstracted by a virtual link, which is characterized by an equivalent delay and power. Thus, the azimuth AoDs $\phi_n^{\mathrm{MT}}(t)$ and the elevation AoDs $\theta_n^{\mathrm{MT}}(t)$ are only related with the first cluster A_n, and the azimuth AoAs $\phi_n^{\mathrm{MR}}(t)$ and the elevation AoAs $\theta_n^{\mathrm{MR}}(t)$ are only related with the last cluster Z_n.

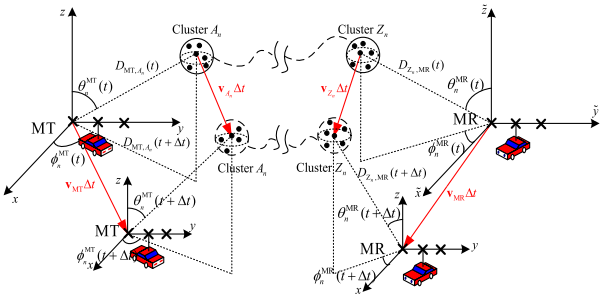

FIGURE 1. MT and MR angle parameters in the 3D non-stationary V2V channel model.

The V2V MIMO channel between the MT and MR in Fig.1 can be expressed as a $U \times S$ complex matrix [30], i.e.,

$$\mathbf{H}(t,\tau) = \begin{bmatrix} h_{1,1}(t,\tau) & h_{1,2}(t,\tau) & \dots & h_{1,S}(t,\tau) \\ h_{2,1}(t,\tau) & h_{u,s}(t,\tau) & \dots & h_{2,S}(t,\tau) \\ \vdots & \vdots & \ddots & \vdots \\ h_{U,1}(t,\tau) & h_{U,2}(t,\tau) & \dots & h_{U,S}(t,\tau) \end{bmatrix} \quad (1)$$

where each element $h_{u,s}(t,\tau)$ denotes the complex channel impulse response (CIR) between the MT antenna element s ($s = 1, 2, \dots, S$) and MR antenna element u ($u = 1, 2, \dots, U$), and it can be expressed as [17]

$$h_{u,s}(t,\tau) = \sum_{n=1}^{N(t)} \sqrt{P_n(t)}\tilde{h}_{u,s,n}(t)\delta(\tau - \tau_n(t)) \quad (2)$$

where $N(t)$ is the number of valid paths, which can be characterized by the path delay $\tau_n(t)$, path power $P_n(t)$, and channel coefficient $\tilde{h}_{u,s,n}(t)$ with normalized power. In this paper, $\tilde{h}_{u,s,n}(t)$ is modeled as the superposition of infinite sub-paths, i.e.,

$$\tilde{h}_{u,s,n}(t) = \lim_{M\to\infty} \sqrt{\frac{1}{M}} \sum_{m=1}^{M} \mathrm{e}^{\mathrm{j}(\Phi_{n,m}^{\mathrm{D}}(t)+\Phi_{n,m}^{\mathrm{L}}(t)+\Phi_{n,m}^{\mathrm{I}})} \quad (3)$$

where M is the number of sub-paths, $\Phi_{n,m}^{\mathrm{I}}$ represents the random initial phase and is usually distributed uniformly over $[0, 2\pi)$. $\Phi_{n,m}^{\mathrm{L}}(t)$ accounts for the phase related with the antenna index and scattering environment, and it can be further expressed as

$$\Phi_{n,m}^{\mathrm{L}}(t) = k\left(\mathbf{d}_s^{\mathrm{MT}} \cdot \mathbf{s}_{n,m}^{\mathrm{MT}}(t) + \mathbf{d}_u^{\mathrm{MR}} \cdot \mathbf{s}_{n,m}^{\mathrm{MR}}(t)\right) \quad (4)$$

where $k = 2\pi f_c/c$ denotes the wave number, and f_c and c represent the carrier frequency and speed of light, respectively. $\mathbf{s}_{n,m}^{\mathrm{MT}}(t)$ and $\mathbf{s}_{n,m}^{\mathrm{MR}}(t)$ are the AoD and AoA unit vectors of the mth sub-path within the nth path, respectively,

$$\mathbf{s}_{n,m}^{\mathrm{MT}}(t) = \begin{bmatrix} \cos\theta_{n,m}^{\mathrm{MT}}(t)\cos\phi_{n,m}^{\mathrm{MT}}(t) \\ \cos\theta_{n,m}^{\mathrm{MT}}(t)\sin\phi_{n,m}^{\mathrm{MT}}(t) \\ \sin\theta_{n,m}^{\mathrm{MT}}(t) \end{bmatrix} \quad (5)$$

$$\mathbf{s}_{n,m}^{\mathrm{MR}}(t) = \begin{bmatrix} \cos\theta_{n,m}^{\mathrm{MR}}(t)\cos\phi_{n,m}^{\mathrm{MR}}(t) \\ \cos\theta_{n,m}^{\mathrm{MR}}(t)\sin\phi_{n,m}^{\mathrm{MR}}(t) \\ \sin\theta_{n,m}^{\mathrm{MR}}(t) \end{bmatrix}. \quad (6)$$

TABLE 1. Definitions of channel parameters.

$N(t)$	number of valid paths
$P_n(t), \tau_n(t)$	power and delay of the nth path, respectively
M	number of sub-paths
$\mathbf{d}_s^{\mathrm{MT}}, \mathbf{d}_u^{\mathrm{MR}}$	location vectors of the transmitting antenna s and receiving antenna u, respectively
$\mathbf{L}^{\mathrm{MT}}(t), \mathbf{L}^{\mathrm{MR}}(t), \mathbf{L}^{A_n}(t), \mathbf{L}^{Z_n}(t)$	location vectors of the MT, MR, A_n, and Z_n at time instant t, respectively
$\mathbf{s}_{n,m}^{\mathrm{MT}}, \mathbf{s}_{n,m}^{\mathrm{MR}}$	departure and arrival angle unit vectors of the mth sub-path within the nth path, respectively
$\phi_n^{\mathrm{MT}}(t), \theta_n^{\mathrm{MT}}(t)$	azimuth and elevation AoDs, respectively
$\phi_n^{\mathrm{MR}}(t), \theta_n^{\mathrm{MR}}(t)$	azimuth and elevation AoAs, respectively
$\mathbf{v}^{\mathrm{MT}}, \mathbf{v}^{\mathrm{MR}}, \mathbf{v}^{A_n}, \mathbf{v}^{\mathrm{Z_n}}$	velocity vectors of the MT, MR, A_n, and Z_n, respectively
$\phi_{\mathbf{v}}^{\mathrm{MT}}, \phi_{\mathbf{v}}^{\mathrm{MR}}, \phi_{\mathbf{v}}^{A_n}, \phi_{\mathbf{v}}^{Z_n}$	azimuth angles of the velocities of MT, MR, A_n, and Z_n, respectively
$\theta_{\mathbf{v}}^{\mathrm{MT}}, \theta_{\mathbf{v}}^{\mathrm{MR}}, \theta_{\mathbf{v}}^{A_n}, \theta_{\mathbf{v}}^{Z_n}$	elevation angles of the velocities of MT, MR, A_n, and Z_n, respectively
$\mathbf{v}^{\mathrm{MT},A_n}, \mathbf{v}^{\mathrm{MR},Z_n}$	relative velocity vectors between MT and A_n, and MR and Z_n, respectively
$\phi_{\mathbf{v}}^{\mathrm{MT},A_n}, \phi_{\mathbf{v}}^{\mathrm{MR},Z_n}$	azimuth angles of the relative velocities between MT and A_n, and MR and Z_n, respectively
$\theta_{\mathbf{v}}^{\mathrm{MT},A_n}, \theta_{\mathbf{v}}^{\mathrm{MR},Z_n}$	elevation angles of the relative velocities between MT and A_n, and MR and Z_n, respectively

$\mathbf{d}_s^{\mathrm{MT}} = [d_{s,x}^{\mathrm{MT}}, d_{s,y}^{\mathrm{MT}}, d_{s,z}^{\mathrm{MT}}]$ and $\mathbf{d}_u^{\mathrm{MR}} = [d_{u,\tilde{x}}^{\mathrm{MR}}, d_{u,\tilde{y}}^{\mathrm{MR}}, d_{u,\tilde{z}}^{\mathrm{MR}}]$ are the location vectors of the transmitting antenna s in the MT coordinate system (xyz) and the receiving antenna u in the MR coordinate system ($\tilde{x}\tilde{y}\tilde{z}$), respectively. In (3), $\Phi_{n,m}^{\mathrm{D}}(t)$ denotes the phase associated with the Doppler frequency and can be further written as

$$\Phi_{n,m}^{\mathrm{D}}(t) = 2\pi \int_0^t f_{n,m}(t)\mathrm{d}t \tag{7}$$

where $f_{n,m}(t)$ represents the Doppler frequency of the mth sub-path within the nth path, and it can be expressed as

$$\begin{aligned} f_{n,m}(t) &= \left[(\mathbf{v}^{\mathrm{MT}} - \mathbf{v}^{A_n}) \cdot \mathbf{s}_{n,m}^{\mathrm{MT}}(t) + (\mathbf{v}^{Z_n} - \mathbf{v}^{\mathrm{MR}}) \cdot \mathbf{s}_{n,m}^{\mathrm{MR}}(t)\right]/\lambda \\ &= \left(\mathbf{v}^{\mathrm{MT},A_n} \cdot \mathbf{s}_{n,m}^{\mathrm{MT}}(t) + \mathbf{v}^{Z_n,\mathrm{MR}} \cdot \mathbf{s}_{n,m}^{\mathrm{MR}}(t)\right)/\lambda \end{aligned} \tag{8}$$

where $\lambda = c/f_c$ is the length of wave, $\mathbf{v}^{\mathrm{MT},A_n}$ denotes the relative velocity between the MT and cluster A_n, and $\mathbf{v}^{Z_n,\mathrm{MR}}$ means the relative velocity between the cluster Z_n and MR. For simplicity, all velocity vectors are assumed unchanged during the short analytical time interval, and they can be expressed as

$$\begin{aligned} &\mathbf{v}^{\mathrm{MT/MR}/A_n/Z_n} \\ &\quad = \left\|\mathbf{v}^{\mathrm{MT/MR}/A_n/Z_n}\right\| \\ &\qquad \cdot \begin{bmatrix} \cos\theta_{\mathbf{v}}^{\mathrm{MT/MR}/A_n/Z_n} \cos\phi_{\mathbf{v}}^{\mathrm{MT/MR}/A_n/Z_n} \\ \cos\theta_{\mathbf{v}}^{\mathrm{MT/MR}/A_n/Z_n} \sin\phi_{\mathbf{v}}^{\mathrm{MT/MR}/A_n/Z_n} \\ \sin\theta_{\mathbf{v}}^{\mathrm{MT/MR}/A_n/Z_n} \end{bmatrix} \end{aligned} \tag{9}$$

$$\mathbf{v}^{\mathrm{MT},A_n} = \left\|\mathbf{v}^{\mathrm{MT},A_n}\right\| \cdot \begin{bmatrix} \cos\theta_{\mathbf{v}}^{\mathrm{MT},A_n} \cos\phi_{\mathbf{v}}^{\mathrm{MT},A_n} \\ \cos\theta_{\mathbf{v}}^{\mathrm{MT},A_n} \sin\phi_{\mathbf{v}}^{\mathrm{MT},A_n} \\ \sin\theta_{\mathbf{v}}^{\mathrm{MT},A_n} \end{bmatrix} \tag{10}$$

$$\mathbf{v}^{Z_n,\mathrm{MR}} = \left\|\mathbf{v}^{Z_n,\mathrm{MR}}\right\| \cdot \begin{bmatrix} \cos\theta_{\mathbf{v}}^{Z_n,\mathrm{MR}} \cos\phi_{\mathbf{v}}^{Z_n,\mathrm{MR}} \\ \cos\theta_{\mathbf{v}}^{Z_n,\mathrm{MR}} \sin\phi_{\mathbf{v}}^{Z_n,\mathrm{MR}} \\ \sin\theta_{\mathbf{v}}^{Z_n,\mathrm{MR}} \end{bmatrix} \tag{11}$$

where $\left\|\mathbf{v}^{\mathrm{MT/MR}/A_n/Z_n}\right\|$, $\phi_{\mathbf{v}}^{\mathrm{MT/MR}/A_n/Z_n}$ and $\theta_{\mathbf{v}}^{\mathrm{MT/MR}/A_n/Z_n}$ denote the amplitudes, the azimuth and elevation angles of $\mathbf{v}^{\mathrm{MT}}$, $\mathbf{v}^{\mathrm{MR}}$, $\mathbf{v}^{A_n}$, and $\mathbf{v}^{Z_n}$, respectively, and $\left\|\mathbf{v}^{\mathrm{MT},A_n}\right\|$, $\phi_{\mathbf{v}}^{\mathrm{MT},A_n}$, $\theta_{\mathbf{v}}^{\mathrm{MT},A_n}$ and $\left\|\mathbf{v}^{Z_n,\mathrm{MR}}\right\|$, $\phi_{\mathbf{v}}^{Z_n,\mathrm{MR}}$, $\theta_{\mathbf{v}}^{Z_n,\mathrm{MR}}$ denote the amplitudes, the azimuth and elevation angles of $\mathbf{v}^{\mathrm{MT},A_n}$ and $\mathbf{v}^{Z_n,\mathrm{MR}}$, respectively. The detailed definitions of channel parameters can be found in Table 1.

B. COMPARISON OF TIME-VARIANT DOPPLER FREQUENCIES

The theoretical Doppler frequency for 3D V2V channels can be derived by combining the methods in [15] and [31] as (12), as shown at the bottom of this page, which is the function of the AoAs, AoDs and the velocity vectors of the MT, MR, and clusters. Compared with the non-stationary V2V channel models (or Class B models) in [13]–[20], we can see that the authors used the following item to represent the phase associated with the time-variant Doppler

$$\begin{aligned} \tilde{f}_{n,m}(t) &= \begin{bmatrix} \left\|\mathbf{v}^{\mathrm{MT}}\right\| \left(\cos(\phi_{\mathbf{v}}^{\mathrm{MT}} - \phi_{n,m}^{\mathrm{MT}}(t)) \cos\theta_{n,m}^{\mathrm{MT}}(t) \cos\theta_{\mathbf{v}}^{\mathrm{MT}} + \sin\theta_{n,m}^{\mathrm{MT}}(t) \sin\theta_{\mathbf{v}}^{\mathrm{MT}}\right) \\ -\left\|\mathbf{v}^{A_n}\right\| \left(\cos(\phi_{n,m}^{\mathrm{MT}}(t) - \phi_{\mathbf{v}}^{A_n}) \cos\theta_{n,m}^{\mathrm{MT}}(t) \cos\theta_{\mathbf{v}}^{A_n} + \sin\theta_{n,m}^{\mathrm{MT}}(t) \sin\theta_{\mathbf{v}}^{A_n}\right) \\ -\left\|\mathbf{v}^{Z_n}\right\| \left(\cos(\phi_{\mathbf{v}}^{Z_n} - \phi_{n,m}^{\mathrm{MR}}(t)) \cos\theta_{n,m}^{\mathrm{MR}}(t) \cos\theta_{\mathbf{v}}^{Z_n} + \sin\theta_{n,m}^{\mathrm{MR}}(t) \sin\theta_{\mathbf{v}}^{Z_n}\right) \\ +\left\|\mathbf{v}^{\mathrm{MR}}\right\| \left(\cos(\phi_{\mathbf{v}}^{\mathrm{MR}} - \phi_{n,m}^{\mathrm{MR}}(t)) \cos\theta_{n,m}^{\mathrm{MR}}(t) \cos\theta_{\mathbf{v}}^{\mathrm{MR}} + \sin\theta_{n,m}^{\mathrm{MR}}(t) \sin\theta_{\mathbf{v}}^{\mathrm{MR}}\right) \end{bmatrix}/\lambda \\ &= \left[(\mathbf{v}^{\mathrm{MT}} - \mathbf{v}^{A_n}) \cdot \mathbf{s}_{n,m}^{\mathrm{MT}}(t) + (\mathbf{v}^{Z_n} - \mathbf{v}^{\mathrm{MR}}) \cdot \mathbf{s}_{n,m}^{\mathrm{MR}}(t)\right]/\lambda \end{aligned} \tag{12}$$

frequency

$$\Phi_{n,m}^{\mathrm{D}}{}'(t) = k\left[(\mathbf{v}^{\mathrm{MT}} - \mathbf{v}^{A_n})\cdot\mathbf{s}_{n,m}^{\mathrm{MT}}(t) + (\mathbf{v}^{Z_n} - \mathbf{v}^{\mathrm{MR}})\cdot\mathbf{s}_{n,m}^{\mathrm{MR}}(t)\right]t. \quad (13)$$

This idea comes from the counterpart of stationary V2V channel models [15], where the Doppler frequency is fixed. In the case of non-stationary V2V channels, according to the relationship between the phase and frequency [31], the output Doppler frequency of these models can be derived as

$$\begin{aligned} f'_{n,m}(t) &= \frac{1}{2\pi}\frac{\mathrm{d}\Phi_{n,m}^{\mathrm{D}}{}'(t)}{\mathrm{d}t} \\ &= [(\mathbf{v}^{\mathrm{MT}} - \mathbf{v}^{A_n})\cdot(\frac{\mathrm{d}\mathbf{s}_{n,m}^{\mathrm{MT}}(t)}{\mathrm{d}t}t + \mathbf{s}_{n,m}^{\mathrm{MT}}(t)) \\ &\quad + (\mathbf{v}^{Z_n} - \mathbf{v}^{\mathrm{MR}})\cdot(\frac{\mathrm{d}\mathbf{s}_{n,m}^{\mathrm{MR}}(t)}{\mathrm{d}t}t + \mathbf{s}_{n,m}^{\mathrm{MR}}(t))]/\lambda \neq \tilde{f}_{n,m}(t) \end{aligned} \quad (14)$$

which does not agree well with the theoretical one. In contrast, we use (7) and (8) instead of (13) to represent the accumulated phase in our proposed model. Thus, the corresponding output Doppler frequency can be proved as

$$\begin{aligned} f_{n,m}(t) &= \frac{1}{2\pi}\frac{\mathrm{d}\Phi_{n,m}^{\mathrm{D}}(t)}{\mathrm{d}t} \\ &= \left[(\mathbf{v}^{\mathrm{MT}} - \mathbf{v}^{A_n})\cdot\mathbf{s}_{n,m}^{\mathrm{MT}}(t) + (\mathbf{v}^{Z_n} - \mathbf{v}^{\mathrm{MR}})\cdot\mathbf{s}_{n,m}^{\mathrm{MR}}(t)\right]/\lambda \end{aligned} \quad (15)$$

which is the same as the theoretical Doppler frequency of (12).

C. COMPUTATION METHODS OF TIME-VARIANT CHANNEL PARAMETERS

The measurement campaigns for V2V channels have demonstrated that the number of valid paths is time-variant due to the movements of the MT, MR and clusters [32]. It means that some clusters will disappear and some new clusters will appear, and this can be modeled as a Markov birth-death process [33]. Let us set the birth and death rates as λ_G and λ_R, and model the evolution of path number as a Markov process. Since the movement of clusters in a realistic environment is random and unknowable, each path has its own survival probability in principle. For simplicity, we use the average survival probability to describe the death process and it can be calculated by [29]

$$P_{\mathrm{r}} = \mathrm{e}^{(-\lambda_R(P_c(\|\mathbf{v}^A\|+\|\mathbf{v}^Z\|)\Delta t+\|\mathbf{v}^{\mathrm{MR}}-\mathbf{v}^{\mathrm{MT}}\|\Delta t))} \quad (16)$$

where P_c denotes the percentage of movement, $\|\mathbf{v}^A\|$ and $\|\mathbf{v}^Z\|$ are the magnitudes of average velocities of cluster A_n and Z_n ($n = 1,\ldots,N$), respectively. In order to keep the average number of valid paths constant, the number of newly generated paths $N_{\mathrm{new}}(t)$ is modeled by a Poisson process with the expectation as

$$\mathrm{E}\{N_{\mathrm{new}}(t)\} = \frac{\lambda_G}{\lambda_R}(1 - P_{\mathrm{r}}). \quad (17)$$

Combining (16) with (17), we can obtain the average path number as

$$\mathrm{E}\{N(t)\} = N(t-\Delta t)P_{\mathrm{r}} + \mathrm{E}\{N_{\mathrm{new}}(t)\} = \frac{\lambda_G}{\lambda_R} \quad (18)$$

which only depends on the parameters of birth and death rates.

For the nth valid path at time instant t, the total delay equals to the summation of the delays of the first bounce, virtual link, and last bounce. It can be calculated by

$$\tau_n(t) = \frac{\|\mathbf{L}^{\mathrm{MT}}(t) - \mathbf{L}^{A_n}(t)\| + \|\mathbf{L}^{\mathrm{MR}}(t) - \mathbf{L}^{Z_n}(t)\|}{c} + \tilde{\tau}_n(t) \quad (19)$$

where $\tilde{\tau}_n(t)$ denotes the equivalent delay of virtual link and it can be updated by the first-order filtering method in [29].

The distributions of azimuth and elevation angles at the MT and the MR are supposed to be the Gaussian and Laplacian in WINNER+ [31] and 3GPP-3D models [34], respectively. In order to make the distribution more universal, based on the measurements, Mammasis and Stewart [35] modeled the angle distribution by the 3D VMF distribution. The VMF distribution is a close model for directional data distributed uniformly with rotational symmetry on the unit hypersphere S^{m-1}. When m is 3, the ordinary sphere usually corresponds to the set of all points embedded in the Euclidean space R^3. For the ordinary sphere, the VMF PDF can be defined as

$$p(\phi,\theta) = \frac{\mathrm{e}^{\kappa\left(\cos\theta\cos\bar{\theta}\cos(\phi-\bar{\phi})+\sin\theta\sin\bar{\theta}\right)}\cos\theta}{(\kappa^{1-m/2})(2\pi)^{m/2}\mathrm{I}_{m/2-1}(\kappa)} \quad (20)$$

where $-\pi \le \phi \le \pi, -\pi/2 \le \theta \le \pi/2$, $\bar{\phi}$ and $\bar{\theta}$ indicate the mean values of the azimuth angle and elevation angle, respectively, and $\mathrm{I}_{m/2-1}(\cdot)$ denotes the modified Bessel function of the first kind and order $m/2-1$, where m is a factor and equals to 3 for the 3D VMF distribution. When $m = 2$, it reduces to the 2D Von Mises (VM) distribution. The shape factor κ is a real-valued parameter that controls the concentration of distribution. To demonstrate the VMF distribution with different parameters intuitively, according to the measured data under the urban macro scenario [35], we set $\bar{\phi} = 130^o, \bar{\theta} = -6^o, \kappa = 10.86$, $\bar{\phi} = 10^o$, $\bar{\theta} = 0^o, \kappa = 27.73$ and $\bar{\phi} = 240^o, \bar{\theta} = 6^o, \kappa = 65$. Fig. 2 plots the scatterers (2000 samples) on the unit sphere in a 3D Euclidean space. As we can see that the larger the value of κ, the higher the density near the mean direction. Moreover, the distribution represents the isotropic scenario for the special case of $\kappa = 0$, while it reduces to a point when $\kappa \to \infty$.

Since κ can be obtained by measurements, the time-variant AoDs and AoAs under the non-stationary scenarios are only determined by $\bar{\phi}(t)$ and $\bar{\theta}(t)$, which are tracked by the following steps in this paper. Firstly, the instantaneous locations of the MT, MR, and clusters A_n, Z_n at time instant $t+\Delta t$ can be

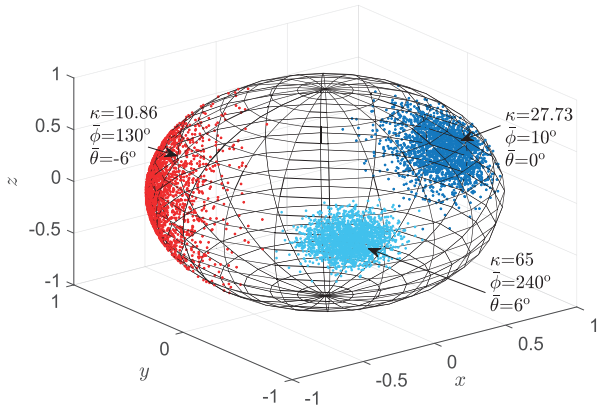

FIGURE 2. The VMF distributions on the unit sphere.

updated by

$$\mathbf{L}^{\mathrm{MT/MR}/A_n/Z_n}(t+\Delta t) = \mathbf{L}^{\mathrm{MT/MR}/A_n/Z_n}(t) + \mathbf{v}^{\mathrm{MT/MR}/A_n/Z_n}\Delta t \tag{21}$$

where $\mathbf{L}^{\mathrm{MT/MR}/A_n/Z_n}(t)$ denote the instantaneous locations of the MT, MR, and clusters A_n, Z_n at time instant t, respectively. Then, the time-variant $\bar{\theta}(t)$ and $\bar{\phi}(t)$ at the MT (MR) in the nth path can be calculated by

$$\bar{\theta}_n^{\mathrm{MT/MR}}(t) = \arcsin\left(\frac{\mathbf{L}_z^{A_n/Z_n}(t) - \mathbf{L}_z^{\mathrm{MT/MR}}(t)}{\left\|\mathbf{L}^{A_n/Z_n}(t) - \mathbf{L}^{\mathrm{MT/MR}}(t)\right\|}\right) \tag{22}$$

$$\bar{\phi}_n^{\mathrm{MT/MR}}(t) = \begin{cases} \arccos\left(\dfrac{\mathbf{L}_x^{A_n/Z_n}(t) - \mathbf{L}_x^{\mathrm{MT/MR}}(t)}{\left(\left\|\mathbf{L}^{A_n/Z_n}(t) - \mathbf{L}^{\mathrm{MT/MR}}(t)\right\|\right)\cos(\bar{\theta}_n^{\mathrm{MT/MR}}(t))}\right), \\ \quad \mathbf{L}_y^{A_n/Z_n}(t) - \mathbf{L}_y^{\mathrm{MT/MR}}(t) \geq 0 \\ -\arccos\left(\dfrac{\mathbf{L}_x^{A_n/Z_n}(t) - \mathbf{L}_x^{\mathrm{MT/MR}}(t)}{\left(\left\|\mathbf{L}^{A_n/Z_n}(t) - \mathbf{L}^{\mathrm{MT/MR}}(t)\right\|\right)\cos(\bar{\theta}_n^{\mathrm{MT/MR}}(t))}\right), \\ \quad \mathbf{L}_y^{A_n/Z_n}(t) - \mathbf{L}_y^{\mathrm{MT/MR}}(t) < 0. \end{cases} \tag{23}$$

III. TIME-VARIANT CORRELATION PROPERTIES FOR THE PROPOSED MODEL

The normalized spatial-temporal correlation function (STCF) between $\tilde{h}_{u_1,s_1,n}(t)$ and $\tilde{h}_{u_2,s_2,n}(t+\Delta t)$ can be defined as [19]

$$\tilde{R}_{u_1,s_1,n}^{u_2,s_2,n}(t;\Delta t,\Delta\mathbf{d}) = \frac{\mathrm{E}\left[\tilde{h}_{u_1,s_1,n}(t)\tilde{h}^*_{u_2,s_2,n}(t+\Delta t)\right]}{\sqrt{\mathrm{E}\left[\left|\tilde{h}_{u_1,s_1,n}(t)\right|^2\right]\mathrm{E}\left[\left|\tilde{h}_{u_2,s_2,n}(t+\Delta t)\right|^2\right]}} \tag{24}$$

where E[·] represents the expectation function, ()* is complex conjugate, Δt is the time lag. The space lag $\Delta\mathbf{d} = \{\Delta\mathbf{d}^{\mathrm{MT}}, \Delta\mathbf{d}^{\mathrm{MR}}\}$ includes the space lag at the MT $\Delta\mathbf{d}^{\mathrm{MT}} = \mathbf{L}_{s_2}^{\mathrm{MT}}(t+\Delta t) - \mathbf{L}_{s_1}^{\mathrm{MT}}(t)$ and the space lag at the MR $\Delta\mathbf{d}^{\mathrm{MR}} = \mathbf{L}_{u_2}^{\mathrm{MR}}(t+\Delta t) - \mathbf{L}_{u_1}^{\mathrm{MR}}(t)$. Substituting our proposed channel model (3) into (24), we can obtain the STCF as (25), as shown at the bottom of this page. As we can see, the time-variant STCF is only related with the time-variant values of AoDs and AoAs when the velocities of both the MT and MR are fixed.

A. TIME-VARIANT SCFS

By setting $\Delta t = 0$, the STCF reduces to the SCF and can be written as

$$\tilde{R}_{u_1s_1,n}^{u_2s_2,n}(t;\Delta\mathbf{d}) = \int_{\{\theta_n^{\mathrm{MT}},\phi_n^{\mathrm{MT}},\theta_n^{\mathrm{MR}},\phi_n^{\mathrm{MR}}\}}\int\int\int\int p(\phi_n^{\mathrm{MT}}(t),\theta_n^{\mathrm{MT}}(t))p(\phi_n^{\mathrm{MR}}(t),\theta_n^{\mathrm{MR}}(t)) \cdot \mathrm{e}^{\mathrm{j}(\Phi^{\mathrm{L}}_{u_2,s_2,n}(t)-\Phi^{\mathrm{L}}_{u_1,s_1,n}(t))}\mathrm{d}\theta_n^{\mathrm{MT}}\mathrm{d}\phi_n^{\mathrm{MT}}\mathrm{d}\theta_n^{\mathrm{MR}}\mathrm{d}\phi_n^{\mathrm{MR}}. \tag{26}$$

Since the clusters A_n and Z_n are independent, we can rewrite (26) as

$$\tilde{R}_{u_1,s_1,n}^{u_2,s_2,n}(t;\Delta\mathbf{d}) = \tilde{R}_n^{\mathrm{MT}}(t;\Delta\mathbf{d}^{\mathrm{MT}})\cdot\tilde{R}_n^{\mathrm{MR}}(t;\Delta\mathbf{d}^{\mathrm{MR}}) \tag{27}$$

where $\tilde{R}_n^{\mathrm{MT}}(t;\Delta\mathbf{d}^{\mathrm{MT}})$ and $\tilde{R}_n^{\mathrm{MR}}(t;\Delta\mathbf{d}^{\mathrm{MR}})$ denote the SCFs at the MT and MR, respectively. Note that the roads are relatively flat under most scenarios. Moreover, since the analytical time interval is very short, i.e., several seconds, it is reasonable to assume that the MT and MR move on the

$$\begin{aligned}\tilde{R}_{u_1,s_1,n}^{u_2,s_2,n}(t;\Delta t,\Delta\mathbf{d}) &= \lim_{M\to\infty}\sqrt{\frac{1}{M}}\sum_{m=1}^{M}\mathrm{e}^{\mathrm{j}(\Phi^{\mathrm{D}}_{u_2,s_2,n,m}(t+\Delta t)+\Phi^{\mathrm{L}}_{u_2,s_2,n,m}(t+\Delta t)+\Phi^{\mathrm{I}}_{n,m})}\mathrm{e}^{-\mathrm{j}(\Phi^{\mathrm{D}}_{u_1,s_1,n,m}(t)+\Phi^{\mathrm{L}}_{u_1,s_1,n,m}(t)+\Phi^{\mathrm{I}}_{n,m})} \\ &= \int_{\{\theta_n^{\mathrm{MT}},\phi_n^{\mathrm{MT}},\theta_n^{\mathrm{MR}},\phi_n^{\mathrm{MR}}\}}\int\int\int\int \sqrt{p(\phi_n^{\mathrm{MT}}(t+\Delta t),\theta_n^{\mathrm{MT}}(t+\Delta t))}\sqrt{p(\phi_n^{\mathrm{MR}}(t+\Delta t),\theta_n^{\mathrm{MR}}(t+\Delta t))}\sqrt{p(\phi_n^{\mathrm{MR}}(t),\theta_n^{\mathrm{MR}}(t))} \\ &\quad\cdot\sqrt{p(\phi_n^{\mathrm{MT}}(t),\theta_n^{\mathrm{MT}}(t))}\mathrm{e}^{\mathrm{j}(\Phi^{\mathrm{D}}_{u_2,s_2,n}(t+\Delta t)-\Phi^{\mathrm{D}}_{u_1,s_1,n}(t)+\Phi^{\mathrm{L}}_{u_2,s_2,n}(t+\Delta t)-\Phi^{\mathrm{L}}_{u_1,s_1,n}(t))}\mathrm{d}\theta_n^{\mathrm{MT}}\mathrm{d}\phi_n^{\mathrm{MT}}\mathrm{d}\theta_n^{\mathrm{MR}}\mathrm{d}\phi_n^{\mathrm{MR}}\end{aligned} \tag{25}$$

$$\tilde{R}_n^{\mathrm{MT}}(t;\Delta\mathbf{d}^{\mathrm{MT}}) = \int_{\{\phi_n^{\mathrm{MT}},\theta_n^{\mathrm{MT}}\}}\int\frac{\cos\theta_n^{\mathrm{MT}}(t)\mathrm{e}^{\kappa\left(\cos\theta_n^{\mathrm{MT}}(t)\cos\bar{\theta}_n^{\mathrm{MT}}(t)\cos(\phi_n^{\mathrm{MT}}(t)-\bar{\phi}_n^{\mathrm{MT}}(t))+\sin\theta_n^{\mathrm{MT}}(t)\sin\bar{\theta}_n^{\mathrm{MT}}(t)\right)}}{(\kappa^{1-m/2})(2\pi)^{m/2}\mathrm{I}_{m/2-1}(\kappa)}\mathrm{e}^{\mathrm{j}k\Delta d_x^{\mathrm{MT}}\cos\phi_n^{\mathrm{MT}}\cos\theta_n^{\mathrm{MT}}}\mathrm{d}\phi_n^{\mathrm{MT}}\mathrm{d}\theta_n^{\mathrm{MT}} \tag{28}$$

horizontal plane during this period. For simplicity, we only consider the case of widely used uniform linear array and set all antenna elements on the x axis. Actually, the following derivation method can be applied to any kinds of antenna arrays. Let us take $\tilde{R}_n^{\mathrm{MT}}(t;\Delta\mathbf{d}^{\mathrm{MT}})$ as an example. By using (4)–(11), $\tilde{R}_n^{\mathrm{MT}}(t;\Delta\mathbf{d}^{\mathrm{MT}})$ under the VMF scattering scenarios can be derived as (28), as shown at the bottom of the previous page. In addition, for the V2V scenarios on the open road, most of non-line-of-sight (NLoS) components occurred are due to the refection of the cars around the MT and MR. Hence, the angle spread on the elevation plane is very small and the VMF distribution is similar with the VM distribution. In this case, $\tilde{R}_n^{\mathrm{MT}}(t;\Delta\mathbf{d}^{\mathrm{MT}})$ can be further simplified as

$$\begin{aligned}&\tilde{R}_n^{\mathrm{MT}}(t;\Delta\mathbf{d}^{\mathrm{MT}})\\&=\int_{-\pi}^{\pi}\frac{\mathrm{e}^{\kappa\cos(\phi_n^{\mathrm{MT}}-\bar{\phi}_n^{\mathrm{MT}}(t))}}{2\pi\mathrm{I}_0(\kappa)}\mathrm{e}^{jk\Delta d_x^{\mathrm{MT}}\cos\phi_n^{\mathrm{MT}}}\mathrm{d}\phi_n^{\mathrm{MT}}\\&=\int_{-\pi}^{\pi}\frac{\mathrm{e}^{(\kappa\cos(\bar{\phi}_n^{\mathrm{MT}}(t))+jk\Delta d_x^{\mathrm{MT}})\cos\phi_n^{\mathrm{MT}}}}{2\pi\mathrm{I}_0(\kappa)}\\&\quad\cdot\mathrm{e}^{\kappa\sin(\bar{\phi}_n^{\mathrm{MT}}(t))\sin\phi_n^{\mathrm{MT}}}\mathrm{d}\phi_n^{\mathrm{MT}}.\end{aligned}\tag{29}$$

Let us set $A(t)=\kappa\sin(\bar{\phi}_n^{\mathrm{MT}}(t))$, $B(t)=\kappa\cos(\bar{\phi}_n^{\mathrm{MT}}(t))+\mathrm{j}k\Delta d_x^{\mathrm{MT}}$ and substitute them into (29), it yields

$$\begin{aligned}&\tilde{R}_n^{\mathrm{MT}}(t;\Delta\mathbf{d}^{\mathrm{MT}})\\&=\frac{1}{2\pi\mathrm{I}_0(\kappa)}\int_{-\pi}^{\pi}\mathrm{e}^{A(t)\sin\phi_n^{\mathrm{MT}}+B(t)\cos\phi_n^{\mathrm{MT}}}\mathrm{d}\phi_n^{\mathrm{MT}}.\end{aligned}\tag{30}$$

By using the integration formula [36, eq. (3.338-4)]

$$\int_{-\pi}^{\pi}\frac{\exp\left[\frac{a+b\sin x+c\cos x}{1+p\sin x+q\cos x}\right]}{1+p\sin x+q\cos x}\mathrm{d}x=\frac{2\pi}{\sqrt{1-p^2-q^2}}\mathrm{e}^{-\alpha}\mathrm{I}_0(\beta)\tag{31}$$

where

$$\alpha=\frac{bp+cq-a}{1-p^2-q^2}\tag{32}$$

$$\beta=\sqrt{\alpha^2-\frac{a^2-b^2-c^2}{1-p^2-q^2}}\tag{33}$$

$$p^2+q^2<1\tag{34}$$

and setting $a=0$, $b=A(t)$, $c=B(t)$, $p=0$, $q=0$, and $x=\phi_n^{\mathrm{MT}}$ into the left side of (31), we can obtain

$$\int_{-\pi}^{\pi}\mathrm{e}^{A(t)\sin\phi_n^{\mathrm{MT}}+B(t)\cos\phi_n^{\mathrm{MT}}}\mathrm{d}\phi_n^{\mathrm{MT}}=2\pi\mathrm{e}^{-\alpha}\mathrm{I}_0(\beta)\tag{35}$$

Then, substituting $\alpha=0$ and $\beta=\sqrt{A^2(t)+B^2(t)}$ into the right hand side of (35), the closed-form expression of (30) can be derived as

$$\begin{aligned}&\tilde{R}_n^{\mathrm{MT}}(t;\Delta\mathbf{d}^{\mathrm{MT}})\\&=\frac{\mathrm{I}_0(\sqrt{\kappa^2+\mathrm{j}2\kappa k\Delta d_x^{\mathrm{MT}}\cos(\bar{\phi}_n^{\mathrm{MT}}(t))-(k\Delta d_x^{\mathrm{MT}})^2})}{\mathrm{I}_0(\kappa)}.\end{aligned}\tag{36}$$

$$\begin{aligned}\tilde{R}_{u,s,n}(t;\Delta t)=P_{\mathrm{r}}\int_{\{\theta_n^{\mathrm{MT}},\phi_n^{\mathrm{MT}},\theta_n^{\mathrm{MR}},\phi_n^{\mathrm{MR}}\}}\int\int\int\mathrm{e}^{\mathrm{j}(\Phi_{u,s,n}^{\mathrm{D}}(t)-\Phi_{u,s,n}^{\mathrm{D}}(t+\Delta t)+\Phi_{u,s,n}^{\mathrm{L}}(t)-\Phi_{u,s,n}^{\mathrm{L}}(t+\Delta t))}\sqrt{p(\phi_n^{\mathrm{MT}}(t+\Delta t),\theta_n^{\mathrm{MT}}(t+\Delta t))}\\\cdot\sqrt{p(\phi_n^{\mathrm{MR}}(t+\Delta t),\theta_n^{\mathrm{MR}}(t+\Delta t))}\sqrt{p(\phi_n^{\mathrm{MT}}(t),\theta_n^{\mathrm{MT}}(t))}\sqrt{p(\phi_n^{\mathrm{MR}}(t),\theta_n^{\mathrm{MR}}(t))}\mathrm{d}\theta_n^{\mathrm{MT}}\mathrm{d}\phi_n^{\mathrm{MT}}\mathrm{d}\theta_n^{\mathrm{MR}}\mathrm{d}\phi_n^{\mathrm{MR}}\end{aligned}\tag{37}$$

$$\begin{aligned}&\tilde{R}_n^{\mathrm{MT}}(t;\Delta t)\\&=\frac{P_{\mathrm{r}}}{(\kappa^{1-m/2})(2\pi)^{m/2}\mathrm{I}_{m/2-1}(\kappa)}\int_{\{\phi_n^{\mathrm{MT}},\theta_n^{\mathrm{MT}}\}}\int\sqrt{\cos\theta_n^{\mathrm{MT}}(t)\mathrm{e}^{\kappa\left(\cos\theta_n^{\mathrm{MT}}(t)\cos\bar{\theta}_n^{\mathrm{MT}}(t)\cos(\phi_n^{\mathrm{MT}}(t)-\bar{\phi}_n^{\mathrm{MT}}(t))+\sin\theta_n^{\mathrm{MT}}(t)\sin\bar{\theta}_n^{\mathrm{MT}}(t)\right)}}\\&\cdot\sqrt{\cos\theta_n^{\mathrm{MT}}(t+\Delta t)\mathrm{e}^{\kappa\left(\cos\theta_n^{\mathrm{MT}}(t+\Delta t)\cos\bar{\theta}_n^{\mathrm{MT}}(t+\Delta t)\cos(\phi_n^{\mathrm{MT}}(t+\Delta t)-\bar{\phi}_n^{\mathrm{MT}}(t+\Delta t))+\sin\theta_n^{\mathrm{MT}}(t+\Delta t)\sin\bar{\theta}_n^{\mathrm{MT}}(t+\Delta t)\right)}}\\&\cdot\mathrm{e}^{\mathrm{j}k\left(d_{s,x}^{\mathrm{MT}}(\cos\phi_n^{\mathrm{MT}}(t)\cos\theta_n^{\mathrm{MT}}(t)-\cos\phi_n^{\mathrm{MT}}(t+\Delta t)\cos\theta_n^{\mathrm{MT}}(t+\Delta t))\right)}\mathrm{e}^{-\mathrm{j}k\int_t^{t+\Delta t}\left\|\mathbf{v}^{\mathrm{MT},A_n}\right\|\left[\cos(\phi_{\mathbf{v}}^{\mathrm{MT},A_n}-\phi_n^{\mathrm{MT}}(t))\cos(\theta_n^{\mathrm{MT}}(t))\right]\mathrm{d}t}\mathrm{d}\phi_n^{\mathrm{MT}}\mathrm{d}\theta_n^{\mathrm{MT}}\end{aligned}\tag{38}$$

$$\begin{aligned}\tilde{R}_n^{\mathrm{MT}}(t;\Delta t)=&\frac{P_{\mathrm{r}}}{(\kappa^{1-m/2})(2\pi)^{m/2}\mathrm{I}_{m/2-1}(\kappa)}\int_{\{\phi_n^{\mathrm{MT}},\theta_n^{\mathrm{MT}}\}}\int\sqrt{\cos\theta_n^{\mathrm{MT}}\mathrm{e}^{\kappa\left(\cos\theta_n^{\mathrm{MT}}\cos\bar{\theta}_n^{\mathrm{MT}}(t)\cos(\phi_n^{\mathrm{MT}}-\bar{\phi}_n^{\mathrm{MT}}(t))+\sin\theta_n^{\mathrm{MT}}\sin\bar{\theta}_n^{\mathrm{MT}}(t)\right)}}\\&\cdot\sqrt{\mathrm{e}^{\kappa\left(\cos(\theta_n^{\mathrm{MT}}+C_\theta^{\mathrm{MT}}(t)\Delta t)\cos(\bar{\theta}_n^{\mathrm{MT}}(t)+C_\theta^{\mathrm{MT}}(t)\Delta t)\cos(\phi_n^{\mathrm{MT}}-\bar{\phi}_n^{\mathrm{MT}}(t))+\sin(\theta_n^{\mathrm{MT}}+C_\theta^{\mathrm{MT}}(t)\Delta t)\sin(\bar{\theta}_n^{\mathrm{MT}}(t)+C_\theta^{\mathrm{MT}}(t)\Delta t)\right)}}\\&\cdot\sqrt{\cos(\theta_n^{\mathrm{MT}}+C_\theta^{\mathrm{MT}}(t)\Delta t)}\mathrm{e}^{-\mathrm{j}k\left\|\mathbf{v}^{\mathrm{MT},A_n}\right\|\left(\begin{array}{l}\frac{\cos\left(-\phi_n^{\mathrm{MT}}+\theta_n^{\mathrm{MT}}+(-C_\phi^{\mathrm{MT}}(t)+C_\theta^{\mathrm{MT}}(t))\Delta t/2+\phi_{\mathbf{v}}^{\mathrm{MT},A_n}\right)\sin\left((-C_\phi^{\mathrm{MT}}(t)+C_\theta^{\mathrm{MT}}(t))\Delta t/2\right)}{(-C_\phi^{\mathrm{MT}}(t)+C_\theta^{\mathrm{MT}}(t))}\\+\frac{\cos\left(-\phi_n^{\mathrm{MT}}-\theta_n^{\mathrm{MT}}-(C_\phi^{\mathrm{MT}}(t)+C_\theta^{\mathrm{MT}}(t))\Delta t/2+\phi_{\mathbf{v}}^{\mathrm{MT},A_n}\right)\sin\left((C_\phi^{\mathrm{MT}}(t)+C_\theta^{\mathrm{MT}}(t))\Delta t/2\right)}{(C_\phi^{\mathrm{MT}}(t)+C_\theta^{\mathrm{MT}}(t))}\end{array}\right)}\\&\cdot\mathrm{e}^{\mathrm{j}kd_{s,x}^{\mathrm{MT}}\left(\cos\phi_n^{\mathrm{MT}}\cos\theta_n^{\mathrm{MT}}-\cos(\phi_n^{\mathrm{MT}}+C_\phi^{\mathrm{MT}}(t)\Delta t)\cos(\theta_n^{\mathrm{MT}}+C_\theta^{\mathrm{MT}}(t)\Delta t)\right)}\mathrm{d}\phi_n^{\mathrm{MT}}\mathrm{d}\theta_n^{\mathrm{MT}}\end{aligned}\tag{39}$$

In a similar way, we can derive the closed-form expression of $\tilde{R}_n^{\mathrm{MR}}(t;\,\Delta\mathbf{d}^{\mathrm{MR}})$ and finally obtain the SCF of the proposed non-stationary V2V channel model. It should be noticed that the SCFs are time dependent due to the time-varying scattering environment.

B. TIME-VARIANT TCFS

By setting $\Delta\mathbf{d} = 0$ in (25), the STCF reduces to the TCF and can be obtained as (37), as shown at the bottom of the previous page. It also equals to the product of TCFs at the MT and MR when the clusters A_n and Z_n are independent. As an example, considering the antenna elements on the x axis and the MT moving on the horizontal plane, the TCF at the MT $\tilde{R}_{\mathrm{MT},n}(t;\,\Delta t)$ can be derived as (38), as shown at the bottom of the previous page.

Since the shape factor κ is fixed during the time interval, the angle offset is also time-invariant, i.e., $\phi_n^{\mathrm{MT}}(t+\Delta t) - \bar{\phi}_n^{\mathrm{MT}}(t+\Delta t) = \phi_n^{\mathrm{MT}}(t) - \bar{\phi}_n^{\mathrm{MT}}(t)$. It's reasonable to assume that the elevation AoDs and azimuth AoDs change linearly during the short time interval as $\phi_n^{\mathrm{MT}}(t+\Delta t) = \phi_n^{\mathrm{MT}}(t) + C_\phi^{\mathrm{MT}}(t)\Delta t$ and $\theta_n^{\mathrm{MT}}(t+\Delta t) = \theta_n^{\mathrm{MT}}(t) + C_\theta^{\mathrm{MT}}(t)\Delta t$, respectively. Therefore, $\tilde{R}_n^{\mathrm{MT}}(t;\,\Delta t)$ can be rewritten as (39), as shown at the bottom of the previous page. Similarly, if we consider the angle spread on the elevation plane is very small, by substituting $m = 2$ and $\bar{\theta}_n^{\mathrm{MT}}(t) = 0$ into (39), it can be simplified as

$$\tilde{R}_n^{\mathrm{MT}}(t;\,\Delta t) = \frac{P_{\mathrm{r}}}{2\pi \mathrm{I}_0(\kappa)} \int_{-\pi}^{\pi} \mathrm{e}^{\kappa\cos(\phi_n^{\mathrm{MT}}(t)-\bar{\phi}_n^{\mathrm{MT}}(t))} \cdot \mathrm{e}^{\mathrm{j}D^{\mathrm{MT}}(t;\,\Delta t)\sin(\phi_n^{\mathrm{MT}}(t)+\frac{C_\phi^{\mathrm{MT}}(t)\Delta t}{2}+E^{\mathrm{MT}}(t;\,\Delta t))}\mathrm{d}\phi_n^{\mathrm{MT}} \tag{40}$$

where

$$D^{\mathrm{MT}}(t;\,\Delta t) = 2k\sin(C_\phi^{\mathrm{MT}}(t)\Delta t/2) \cdot \sqrt{{d_{s,x}^{\mathrm{MT}}}^2 + \left(\frac{\left\|\mathbf{v}^{\mathrm{MT},A_n}\right\|}{C_\phi^{\mathrm{MT}}(t)}\right)^2 - \frac{2d_{s,x}^{\mathrm{MT}}\sin(\phi_{\mathbf{v}}^{\mathrm{MT},A_n})\left\|\mathbf{v}^{\mathrm{MT},A_n}\right\|}{C_\phi^{\mathrm{MT}}(t)}} \tag{41}$$

$$E^{\mathrm{MT}}(t;\,\Delta t) = \arctan\left(\frac{\left\|\mathbf{v}^{\mathrm{MT},A_n}\right\|/C_\phi^{\mathrm{MT}}(t)\cos(\phi_{\mathbf{v}}^{\mathrm{MT},A_n})}{\left\|\mathbf{v}^{\mathrm{MT},A_n}\right\|/C_\phi^{\mathrm{MT}}(t)\sin(\phi_{\mathbf{v}}^{\mathrm{MT},A_n}) - d_{s,x}^{\mathrm{MT}}}\right). \tag{42}$$

Finally, by using the integration formula [36, eq. (3.338-4)], the closed-form expression of $\tilde{R}_n^{\mathrm{MT}}(t;\,\Delta t)$ can be derived as

$$\tilde{R}_n^{\mathrm{MT}}(t;\,\Delta t) = \frac{P_{\mathrm{r}}\mathrm{I}_0(\sqrt{\kappa^2 - {D^{\mathrm{MT}}}^2(t;\,\Delta t) + F^{\mathrm{MT}}(t;\,\Delta t)})}{\mathrm{I}_0(\kappa)} \tag{43}$$

where

$$F^{\mathrm{MT}}(t;\,\Delta t) = 2\mathrm{j}\kappa D^{\mathrm{MT}}(t;\,\Delta t) \cdot \sin\left(\bar{\phi}_n^{\mathrm{MT}}(t) + C_\phi^{\mathrm{MT}}(t)\Delta t/2 + E^{\mathrm{MT}}(t;\,\Delta t)\right). \tag{44}$$

In a similar way, the TCFs at the MR and the proposed channel model can also be obtained.

IV. SIMULATION RESULTS AND VALIDATION

In this section, we compare the simulation results with the theoretical and measured results. In the simulation, the MT and MR are both equipped with linear antenna arrays. The first antenna elements of the MT and MR are located at the coordinate origins, respectively. Both the AoA and AoD are assumed to follow the VMF distributions with $\kappa = 27.73$ [35], and the clusters distribute uniformly in the propagation area. Based on the measurement scenario in [26], we set the speeds of clusters A_n and Z_n as the Gaussian distribution with the mean value and variance of 1 km/h and 0.1, respectively. In addition, $\phi_{\mathbf{v}}^{A_n}$ and $\phi_{\mathbf{v}}^{Z_n}$ follow the uniform distribution over 0 and 2π, and $\theta_{\mathbf{v}}^{A_n}$ and $\theta_{\mathbf{v}}^{Z_n}$ follow the uniform distribution between $-\pi/36$ and $\pi/36$. The detailed simulation parameters are listed in Table 2.

TABLE 2. The detailed simulation parameters.

M	1000	κ	27.73
λ_G (m^{-1})	0.8	λ_R (m^{-1})	0.04
f_c (GHz)	2.4	$D^{\mathrm{MT,MR}}(t_0)$ (m)	100
$\mathbf{L}^{\mathrm{MT}}(t_0)$ (m)	[0, 0, 0]	$\left\|\mathbf{v}^{\mathrm{MT}}\right\|$ (km/h)	20
$\mathbf{L}^{\mathrm{MR}}(t_0)$ (m)	[0, 0, 0]	$\left\|\mathbf{v}^{\mathrm{MR}}\right\|$ (km/h)	40
$\mathbf{L}^{A_n}(t_0)$ (m)	[20, -60, 1]	$\left\|\mathbf{v}^{A_n}\right\|$ (km/h)	1
$\mathbf{L}^{Z_n}(t_0)$ (m)	[20, 40, 1]	$\left\|\mathbf{v}^{Z_n}\right\|$ (km/h)	1
$\phi_{\mathbf{v}}^{\mathrm{MT}}$	$2\pi/5$	$\theta_{\mathbf{v}}^{\mathrm{MT}}$	0
$\phi_{\mathbf{v}}^{\mathrm{MR}}$	$-3\pi/5$	$\theta_{\mathbf{v}}^{\mathrm{MR}}$	0
$\phi_{\mathbf{v}}^{A_n}$	$2\pi/5$	$\theta_{\mathbf{v}}^{A_n}$	0
$\phi_{\mathbf{v}}^{Z_n}$	$2\pi/5$	$\theta_{\mathbf{v}}^{Z_n}$	0

Firstly, we use (21)–(23) to track the time-variant AoDs and AoAs of the nth path, respectively. The instantaneous PDFs of AoDs and AoAs at three time instants, i.e., t = 0 s, 5 s, and 10 s, are given in Fig. 3, which clearly shows the time varying processes of both the AoDs and AoAs. Then, by substituting the time-variant angles and the velocity vectors into (7) and (8), the output phase within the mth sub-path is obtained and given in Fig. 4. According to the relationship between the phase and frequency, the output Doppler frequency within the mth sub-path is also calculated and shown in Fig. 4. For comparison purpose, the corresponding output phases and Doppler frequencies of conventional non-stationary V2V channel models [13]–[20] as well as the theoretical Doppler frequency calculated by (12) are also given in Fig. 4. As we can see that the output phases of two kinds of models are different, which would lead to different Doppler frequencies as demonstrated in Section II. B. Moreover, the Doppler frequency of our proposed model is much closer to the theoretical one.

To verify the spatial and temporal correlation properties of our proposed model, we compare the theoretical and simulated SCFs and TCFs at three time instants, i.e., $t = 0$ s,

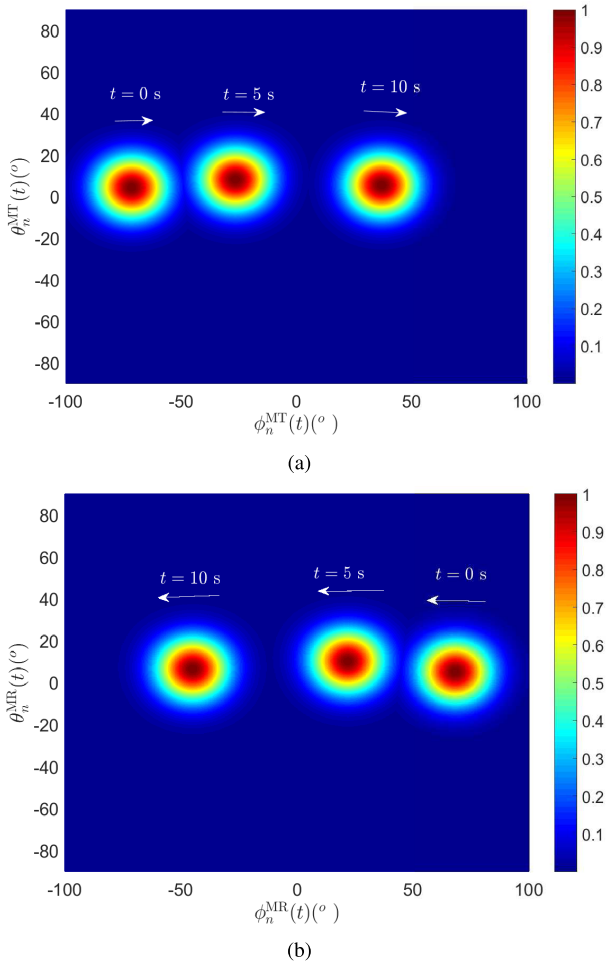

FIGURE 3. Time-variant (a) AoDs and (b) AoAs of the nth path at different time instants under the VMF scattering scenario ($f_c = 2.4$ GHz, $\mathbf{L}^{\mathrm{MT}}(t_0) = [0, 0, 0]$ m, $\mathbf{L}^{\mathrm{MR}}(t_0) = [0, 0, 0]$ m, $\mathbf{L}^{An}(t_0) = [20, -60, 1]$ m, $\mathbf{L}^{Zn}(t_0) = [20, 40, 1]$ m, $D^{\mathrm{MT,MR}}(t_0) = 100$ m, $\|\mathbf{v}^{\mathrm{MT}}\| = 20$ km/h, $\|\mathbf{v}^{\mathrm{MR}}\| = 40$ km/h, $\|\mathbf{v}^{An}\| = 1$ km/h, $\|\mathbf{v}^{Zn}\| = 1$ km/h, $\phi_{\mathbf{v}}^{\mathrm{MT}} = 2\pi/5$, $\phi_{\mathbf{v}}^{\mathrm{MR}} = -3\pi/5$, $\phi_{\mathbf{v}}^{An} = 2\pi/5$, $\phi_{\mathbf{v}}^{Zn} = 2\pi/5$, $\theta_{\mathbf{v}}^{\mathrm{MT}} = \theta_{\mathbf{v}}^{\mathrm{MR}} = \theta_{\mathbf{v}}^{An} = \theta_{\mathbf{v}}^{Zn} = 0$).

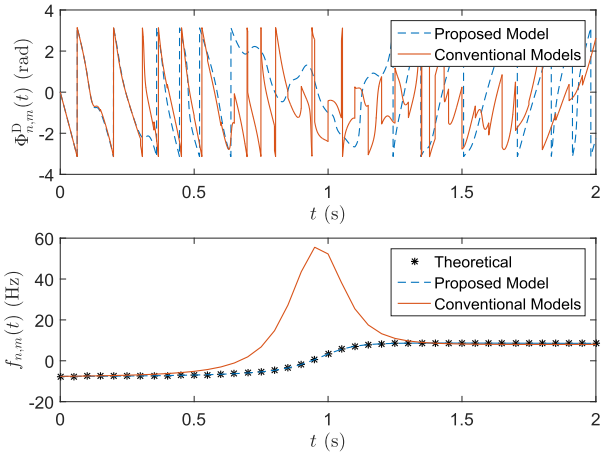

FIGURE 4. Phases and Doppler frequencies of the proposed model and conventional non-stationary models [13]–[20] ($f_c = 2.4$ GHz, $\mathbf{L}^{\mathrm{MT}}(t_0) = [0, 0, 0]$ m, $\mathbf{L}^{\mathrm{MR}}(t_0) = [0, 0, 0]$ m, $\mathbf{L}^{An}(t_0) = [20, -60, 1]$ m, $\mathbf{L}^{Zn}(t_0) = [20, 40, 1]$ m, $D^{\mathrm{MT,MR}}(t_0) = 100$ m, $\|\mathbf{v}^{\mathrm{MT}}\| = 20$ km/h, $\|\mathbf{v}^{\mathrm{MR}}\| = 40$ km/h, $\|\mathbf{v}^{An}\| = 1$ km/h, $\|\mathbf{v}^{Zn}\| = 1$ km/h, $\phi_{\mathbf{v}}^{\mathrm{MT}} = 2\pi/5$, $\phi_{\mathbf{v}}^{\mathrm{MR}} = -3\pi/5$, $\phi_{\mathbf{v}}^{An} = 2\pi/5$, $\phi_{\mathbf{v}}^{Zn} = 2\pi/5$, $\theta_{\mathbf{v}}^{\mathrm{MT}} = \theta_{\mathbf{v}}^{\mathrm{MR}} = \theta_{\mathbf{v}}^{An} = \theta_{\mathbf{v}}^{Zn} = 0$).

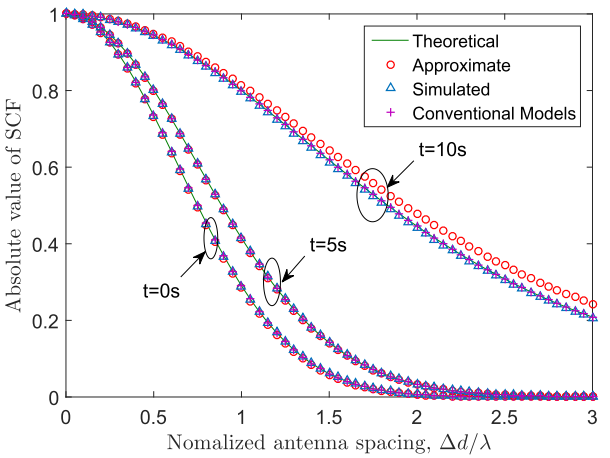

FIGURE 5. Absolute values of the theoretical, approximate, and simulated SCFs of our proposed model at different time instants under the VMF scatteri- ng scenario ($f_c = 2.4$ GHz, $D^{\mathrm{MT,MR}}(t_0) = 100$ m, $\mathbf{L}^{\mathrm{MT}}(t_0) = [0, 0, 0]$ m, $\mathbf{L}^{\mathrm{MR}}(t_0) = [0, 0, 0]$ m, $\mathbf{L}^{An}(t_0) = [20, -60, 1]$ m, $\mathbf{L}^{Zn}(t_0) = [20, 40, 1]$ m, $\|\mathbf{v}^{\mathrm{MT}}\| = 20$ km/h, $\|\mathbf{v}^{\mathrm{MR}}\| = 40$ km/h, $\|\mathbf{v}^{An}\| = 1$ km/h, $\|\mathbf{v}^{Zn}\| = 1$ km/h, $\phi_{\mathbf{v}}^{\mathrm{MT}} = 2\pi/5$, $\phi_{\mathbf{v}}^{\mathrm{MR}} = -3\pi/5$, $\phi_{\mathbf{v}}^{An} = 2\pi/5$, $\phi_{\mathbf{v}}^{Zn} = 2\pi/5$, $\theta_{\mathbf{v}}^{\mathrm{MT}} = \theta_{\mathbf{v}}^{\mathrm{MR}} = \theta_{\mathbf{v}}^{An} = \theta_{\mathbf{v}}^{Zn} = 0$).

5 s, and 10 s, in Fig. 5 and Fig. 6, respectively. In Fig. 5, the antenna spaces at the MT and MR are the same, and the axis denotes the antenna spacing normalized by the half wavelength. The absolute values of the theoretical and approximated SCFs are calculated by (28) and (36), respectively, with $u_1 = s_1 = 1, u_2 = s_2 = 2$, and $n = 1$. It is noticed that the simulated result agrees well with the theoretical and approximated ones, showing the correctness of both derivation and simulation. Moreover, since the cross-correlation of the received signals by different antennas will degrade the performance of MIMO systems, these theoretical results can help us to optimize the layout of antenna arrays.

In Fig. 6, the absolute values of the theoretical and approximate TCFs are obtained by (38) and (43), respectively, with $u = s = 1$ and $n = 1$. For comparison purpose, the simulated TCFs of other conventional non-stationary models [13]–[20] as well as the measured result [26] are also plotted in Fig. 6. It shows that the simulated TCF of our model fits well to the corresponding theoretical and approximated results, which verifies the theoretical derivations as well as simulations. In addition, the TCF of our proposed model is more closer to the measured one than those of other models.

Finally, the CCDF of stationary interval for the proposed model is also compared with the conventional non-stationary models [13]–[20] and the measurement result [27] in Fig. 7. In the figure, the ordinate values are the probabilities of the stationary intervals larger than the abscissa values. As we can see, the stationary interval of the proposed channel model is

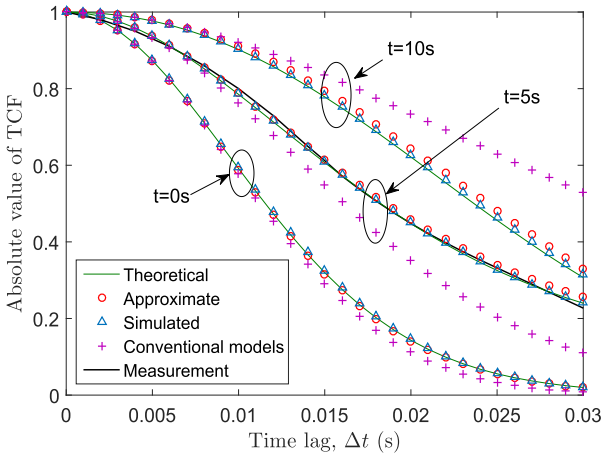

FIGURE 6. Absolute values of the theoretical, approximate, and simulated TCFs of our proposed model, the simulated TCF of conventional non-stati- onary models [13]–[20] at different time instants under the VMF scattering scenario, and the measurement result [26] ($\lambda_G = 0.8$/m, $\lambda_R = 0.04$/m, $f_c = 2.4$ GHz, $D^{\mathrm{MT,MR}}(t_0) = 100$ m, $\mathbf{L}^{\mathrm{MT}}(t_0) = [0, 0, 0]$ m, $\mathbf{L}^{\mathrm{MR}}(t_0) = [0, 0, 0]$ m, $\mathbf{L}^{An}(t_0) = [20, -60, 1]$ m, $\mathbf{L}^{Zn}(t_0) = [20, 40, 1]$ m, $\|\mathbf{v}^{\mathrm{MT}}\| = 20$ km/h, $\|\mathbf{v}^{\mathrm{MR}}\| = 40$ km/h, $\|\mathbf{v}^{An}\| = 1$ km/h, $\|\mathbf{v}^{Zn}\| = 1$ km/h, $\phi_{\mathbf{v}}^{\mathrm{MT}} = 2\pi/5$, $\phi_{\mathbf{v}}^{\mathrm{MR}} = -3\pi/5$, $\phi_{\mathbf{v}}^{An} = 2\pi/5$, $\phi_{\mathbf{v}}^{Zn} = 2\pi/5$, $\theta_{\mathbf{v}}^{\mathrm{MT}} = \theta_{\mathbf{v}}^{\mathrm{MR}} = \theta_{\mathbf{v}}^{An} = \theta_{\mathbf{v}}^{Zn} = 0$).

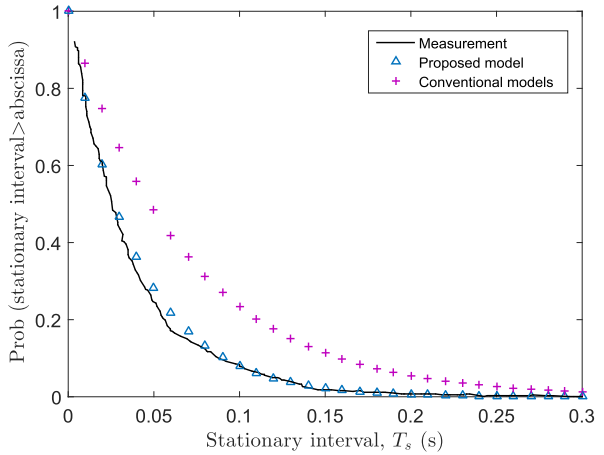

FIGURE 7. The empirical complementary cumulative distribution functions (CCDFs) of stationary intervals for our proposed model, conventional non- stationary models [13]–[20] and measured channel [27] ($\lambda_G = 0.8$ /m, $\lambda_R = 0.04$/m, $f_c = 2.4$ GHz, SampleDensity $= 4$, $c_{thresh} = 0.8$, $D^{\mathrm{MT,MR}}(t_0) = 100$ m, $\mathbf{L}^{\mathrm{MT}}(t_0) = [0, 0, 0]$ m, $\mathbf{L}^{\mathrm{MR}}(t_0) = [0, 0, 0]$ m, $\mathbf{L}^{An}(t_0) = [20, -60, 1]$ m, $\mathbf{L}^{Zn}(t_0) = [20, 40, 1]$ m, $\|\mathbf{v}^{\mathrm{MT}}\| = 20$ km/h, $\|\mathbf{v}^{\mathrm{MR}}\| = 40$ km/h, $\|\mathbf{v}^{An}\| = 1$ km/h, $\|\mathbf{v}^{Zn}\| = 1$ km/h, $\phi_{\mathbf{v}}^{\mathrm{MT}} = 2\pi/5$, $\phi_{\mathbf{v}}^{\mathrm{MR}} = -3\pi/5$, $\phi_{\mathbf{v}}^{An} = 2\pi/5$, $\phi_{\mathbf{v}}^{Zn} = 2\pi/5$, $\theta_{\mathbf{v}}^{\mathrm{MT}} = \theta_{\mathbf{v}}^{\mathrm{MR}} = \theta_{\mathbf{v}}^{An} = \theta_{\mathbf{v}}^{Zn} = 0$).

almost the same as the measurement data, while the conventional non-stationary models tends to have shorter stationary intervals.

V. CONCLUSIONS

In this paper, we have proposed a new 3D non-stationary GBSM for V2V channels with more accurate Doppler frequency. Based on the proposed model, the theoretical expressions of the TCF and SCF under the VMF scattering environment have been derived and verified by simulations. In addition, the TCF and the stationary interval of our proposed model have shown better agreement with the measured results [26] and [27] than those of the existing non-stationary V2V channel models. The new model and the derived theoretical results are very helpful for the realistic performance evaluation and optimization of V2V communication systems.

REFERENCES

[1] X. Cheng *et al.*, "Cooperative MIMO channel modeling and multi-link spatial correlation properties," *IEEE J. Sel. Areas Commun.*, vol. 30, no. 2, pp. 388–396, Feb. 2012.

[2] Q. Zhu, C. Xue, X. Chen, and Y. Yang, "A new MIMO channel model incorporating antenna effects," *Prog. Electromagn. Res. M*, vol. 50, pp. 129–140, Sep. 2016.

[3] J. Zhou, H. Jiang, and H. Kikuchi, "Generalized 3D scattering channel model with MIMO antenna systems," *China Commun.*, vol. 13, no. 5, pp. 66–81, May 2016.

[4] Q. Wu, G. Ding, J. Wang, and Y. D. Yao, "Spatial-temporal opportunity detection for spectrum-heterogeneous cognitive radio networks: Two-dimensional sensing," *IEEE Trans. Wireless Commun.*, vol. 12, no. 2, pp. 516–526, Feb. 2013.

[5] C.-X. Wang, S. Wu, L. Bai, X. You, J. Wang, and C.-L. I, "Recent advances and future challenges for massive MIMO channel measurements and models," *Sci. China Inf. Sci.*, vol. 59, no. 2, pp. 1–16, Feb. 2016.

[6] X. Ge, S. Tu, G. Mao, and C. X. Wang, "5G ultra-dense cellular networks," *IEEE Trans. Wireless Commun.*, vol. 23, no. 1, pp. 72–79, Feb. 2016.

[7] S. Wu, C.-X. Wang, H. M. Aggoune, M. M. Alwakeel, and X. You, "A general 3-D non-stationary 5G wireless channel model," *IEEE Trans. Commun.*, vol. 66, no. 7, pp. 3065–3078, Jul. 2018.

[8] A. G. Zajic and G. L. Stuber, "Space-time correlated mobile-to-mobile channels: Modelling and simulation," *IEEE Trans. Veh. Technol.*, vol. 57, no. 2, pp. 715–726, Mar. 2008.

[9] X. Cheng, C.-X. Wang, D. I. Laurenson, S. Salous, and A. V. Vasilakos, "An adaptive geometry-based stochastic model for non-isotropic MIMO mobile-to-mobile channels," *IEEE Trans. Wireless Commun.*, vol. 8, no. 9, pp. 4824–4835, Sep. 2009.

[10] J. Karedal *et al.*, "A geometry-based stochastic MIMO model for vehicle-to-vehicle communications," *IEEE Trans. Wireless Commun.*, vol. 8, no. 7, pp. 3646–3657, Jul. 2009.

[11] A. Paier *et al.*, "Non-WSSUS vehicular channel characterization in highway and urban scenarios at 5.2 GHz using the local scattering function," in *Proc. Int. ITG WSA*, Darmstadt, Germany, Feb. 2008, pp. 9–15.

[12] R. He *et al.*, "Characterization of quasi-stationarity regions for vehicle-to-vehicle radio channels," *IEEE Trans. Antenna Propag.*, vol. 63, no. 5, pp. 2237–2251, May 2015.

[13] A. Chelli and M. Patzold, "A non-stationary MIMO vehicle-to-vehicle channel model derived from the geometrical street model," in *Proc. IEEE Veh. Technol. Conf. (VTC Fall)*, San Francisco, CA, USA, Sep. 2011, pp. 1–6.

[14] C. A. Gutiérrez, J. T. Gutiérrez-Mena, J. M. Luna-Rivera, D. U. Campos-Delgado, R. Velázquez, and M. Pätzold, "Geometry-based statistical modeling of non-WSSUS mobile-to-mobile Rayleigh fading channels," *IEEE Trans. Veh. Technol.*, vol. 67, no. 1, pp. 362–377, Jan. 2018, doi: 10.1109/TVT.2017.2737952.

[15] A. Borhani and M. Pätzold, "Correlation and spectral properties of vehicle-to-vehicle channels in the presence of moving scatterers," *IEEE Trans. Veh. Technol.*, vol. 62, no. 9, pp. 4228–4239, Sep. 2013.

[16] Y. Bi, J. Zhang, M. Zeng, M. Liu, and X. Xu, "A novel 3D nonstationary channel model based on the von Mises-Fisher scattering distribution," *Mobile Inf. Syst.*, pp. 1–9, Mar. 2016, Art. no. 2161460.

[17] Y. Yuan, C.-X. Wang, Y. He, and M. M. Alwakeel, "3D wideband non-stationary geometry-based stochastic models for non-isotropic MIMO vehicle-to-vehicle channels," *IEEE Trans. Wireless Commun.*, vol. 14, no. 12, pp. 6883–6895, Jul. 2015.

[18] X. Liang, X. Zhao, S. Li, Q. Wang, and W. Lu, "A 3D geometry-based scattering model for vehicle-to-vehicle wideband MIMO relay-based cooperative channels," *China Commun.*, vol. 13, no. 13, pp. 1–10, Oct. 2016.

[19] A. G. Zajić, "Impact of moving scatterers on vehicle-to-vehicle narrowband channel characteristics," *IEEE Trans. Veh. Technol.*, vol. 63, no. 7, pp. 3094–3106, Sep. 2014.
[20] D. Du, X. Zeng, X. Jian, L. Miao, and H. Wang, "Three-dimensional vehicle-to-vehicle channel modeling with multiple moving scatterers," *Mobile Inf. Syst.*, pp. 1–14, May 2017, Art. no. 7231417.
[21] Q. Zhu, X. Liu, X. Yin, X. Chen, and C. Xue, "A novel simulator of non-stationary random mimo channels in Rayleigh fading scenarios," *Int. J. Antennas Propag.*, pp. 1–9, Aug. 2016, Art.no. 3492591.
[22] Q. Zhu *et al.*, "A novel 3D non-stationary wireless MIMO channel simulator and hardware emulator," *IEEE Trans. Wireless Commun.*, pp. 1–14, Apr. 2018, doi: 10.1109/TCOMM.2018.2824817.
[23] A. Borhani, G. L. Stüber, and M. Pätzold, "A random trajectory approach for the development of nonstationary channel models capturing different scales of fading," *IEEE Trans. Veh. Technol.*, vol. 66, no. 1, pp. 2–14, Jan. 2017.
[24] M. Pätzold, C. A. Gutierrez, and N. Youssef, "On the consistency of non-stationary multipath fading channels with respect to the average Doppler shift and the Doppler spread," in *Proc. IEEE Wireless Commun. Netw. Conf. (WCNC)*, San Francisco, CA, USA, Mar. 2017, pp. 1–6.
[25] W. Dahech, M. Pätzold, C. A. Gutiérrez, and N. Youssef, "A non-stationary mobile-to-mobile channel model allowing for velocity and trajectory variations of the mobile stations," *IEEE Trans. Wireless Commun.*, vol. 16, no. 3, pp. 1987–2000, Mar. 2017.
[26] A. Fayziyev, M. Pätzold, E. Masson, Y. Cocheril, and M. Berbineau, "A measurement-based channel model for vehicular communications in tunnels," in *Proc. IEEE Wireless Commun. Netw. Conf. (WCNC)*, Istanbul, Turkey, Apr. 2014, pp. 116–121.
[27] B. Chen, Z. Zhong, and B. Ai, "Stationarity intervals of time-variant channel in high speed railway scenario," *China Commun.*, vol. 9, no. 8, pp. 64–70, Aug. 2012.
[28] H. Hofstertter, A. F. Molisch, and N. Czink, "A twin-cluster MIMO channel model," in *Proc. EuCAP*, Nice, France, Nov. 2006, pp. 1–8.
[29] S. Wu, C.-X. Wang, H. M. Aggoune, M. M. Alwakeel, and Y. He, "A non-stationary 3-D wideband twin-cluster model for 5G massive MIMO channels," *IEEE J. Sel. Areas Commun.*, vol. 32, no. 6, pp. 1207–1218, Jun. 2014.
[30] G. D. Durgin, *Space-Time Wireless Channels*. Upper Saddle River, NJ, USA: Prentice-Hall, 2002.
[31] P. Heino *et al.* (Jun. 2010). *CP5-026 WINNER+ D5.3 V1.0 WINNER+ Final Channel Models*. [Online]. Available: http://projects.celtic-initiative.org/winner+/
[32] I. Sen and D. W. Matolak, "Vehicle–vehicle channel models for the 5-GHz band," *IEEE Trans. Intell. Transp. Syst.*, vol. 9, no. 2, pp. 235–245, Jun. 2008.
[33] T. Zwick, C. Fischer, D. Didascalou, and W. Wiesbeck, "A stochastic spatial channel model based on wave-propagation modeling," *IEEE J. Sel. Areas Commun.*, vol. 18, no. 1, pp. 6–15, Jan. 2000.
[34] *Study on 3D Channel Model for LTE, V12.7.0*, document TR 36.873, 3GPP, Dec. 2017. [Online]. Available: http://www.tech-invite.com/3m36/tinv-3gpp-36-873.html
[35] K. Mammasis and R. W. Stewart, "The Fisher–Bingham spatial correlation model for multielement antenna systems," *IEEE Trans. Veh. Technol.*, vol. 58, no. 5, pp. 2130–2136, Jun. 2009.
[36] I. S. Gradshteyn and I. M. Ryzhik, *Table of Integrals, Series, and Products*. New York, NY, USA: Academic, 2014.

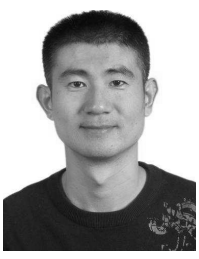

QIUMING ZHU received the B.S. degree in electronic engineering from the Nanjing University of Aeronautics and Astronautics, Nanjing, China, in 2002, and the M.S. and Ph.D. degrees in communication and information systems in 2005 and 2012, respectively. Since 2012, he has been an Associate Professor in wireless communications. From 2016 to 2017, he was also a Visiting Academic at Heriot-Watt University. His research interests include channel modeling for 5G communication systems and wireless channel emulators.

YING YANG received the B.S. degree in information engineering from the Nanjing University of Aeronautics and Astronautics, Nanjing, China, in 2016, where she is currently pursuing the M.S. degree in electronic and communication engineering. Her research interests include the MIMO channel models and channel measurements.

XIAOMIN CHEN received the B.S. degree in electronic engineering and the M.S. and Ph.D. degrees in communication and information systems from the Nanjing University of Aeronautics and Astronautics (NUAA), Nanjing, China, in 1997, 2001, and 2010, respectively. Since 2010, she has been an Associate Professor with NUAA. Her research interests include adaptive techniques for next-generation mobile communication systems and MIMO channel models.

YI TAN received the M.Sc. degree in wireless communication from Lund University, Sweden, in 2012. He is currently pursuing the Ph.D. degree with Heriot-Watt University, Edinburgh, U.K. Before and after his M.Sc. studies, he worked in the industry for a few years related to embedded systems, mobile phone antenna, and firmware of radio chip. He was a Research Assistant with Lund University in 2010 and with Aalborg University from 2014 to 2015.

YU FU received the B.Sc. degree in computer science from Huaqiao University, Fujian, China, in 2009, and the M.Sc. degree in information technology (mobile communications) and the Ph.D. degree in wireless communications from Heriot-Watt University, Edinburgh, U.K., in 2010 and 2015, respectively. He has been a Post-Doctoral Research Associate with Heriot-Watt University since 2015. His main research interests include advanced MIMO communication technologies, wireless channel modeling and simulation, RF tests, and software-defined networks.

CHENG-XIANG WANG (S'01–M'05–SM'08–F'17) received the B.Sc. and M.Eng. degrees in communication and information systems from Shandong University, China, in 1997 and 2000, respectively, and the Ph.D. degree in wireless communications from Aalborg University, Denmark, in 2004.

He was a Research Assistant with the Hamburg University of Technology, Hamburg, Germany, from 2000 to 2001, a Research Fellow with the University of Agder, Grimstad, Norway, from 2001 to 2005, and a Visiting Researcher with Siemens AG, Munich, Germany, in 2004. He has been with Heriot-Watt University, Edinburgh, U.K., since 2005, and became a Professor in wireless communications in 2011. In 2018, he joined Southeast University, China, as a Professor and a Thousand Talent Plan Expert. He has co-authored two books, one book chapter, and over 330 papers in refereed journals and conference proceedings. His current research interests include wireless channel measurements/modeling and (B)5G wireless communication networks, including green communication, cognitive radio networks, high mobility communication networks, massive MIMO, millimeter-wave communication, and visible-light communication.

Dr. Wang is a fellow of IET and HEA. He received nine Best Paper Awards from IEEE GLOBECOM 2010, IEEE ICCT 2011, ITST 2012, IEEE VTC 2013-Spring, IWCMC 2015, IWCMC 2016, IEEE/CIC ICCC 2016, and WPMC 2016. He has served as a technical program committee (TPC) member, the TPC chair, and a general chair for over 80 international conferences. He has served as an Editor for nine international journals, including the IEEE TRANSACTIONS ON WIRELESS COMMUNICATIONS from 2007 to 2009, the IEEE TRANSACTIONS ON VEHICULAR TECHNOLOGY since 2011, and the IEEE TRANSACTIONS ON COMMUNICATIONS since 2015. He was a Lead Guest Editor of the IEEE JOURNAL ON SELECTED AREAS IN COMMUNICATIONS special issue on Vehicular Communications and Networks. He was also a Guest Editor of the IEEE JOURNAL ON SELECTED AREAS IN COMMUNICATIONS special issue on Spectrum and Energy Efficient Design of Wireless Communication Networks and special issue on Airborne Communication Networks, and the IEEE TRANSACTIONS ON BIG DATA special issue on Wireless Big Data. He is recognized as a Web of Science 2017 Highly Cited Researcher.

WEIDONG LI received the B.S. degree in electronic information science and technology from Nanjing Agricultural University, Nanjing, China, in 2017. He is currently pursuing the M.S. degree in signal and information processing with the Nanjing University of Aeronautics and Astronautics. His research interests include MIMO channel models and channel measurements.